Divalent Cation and Ionic Strength Effects on *Vinca* Alkaloid-Induced Tubulin Self-Association

Sharon Lobert,* Coleman A. Boyd,# and John J. Correia#
*School of Nursing and #Department of Biochemistry, University of Mississippi Medical Center, Jackson, Mississippi 39216 USA

ABSTRACT We present here a systematic study of ionic strength and divalent cation effects on *Vinca* alkaloid-induced tubulin spiral formation. We used sedimentation velocity experiments and quantitative fitting of weight-average sedimentation coefficients versus free drug concentrations to obtain thermodynamic parameters under various solution conditions. The addition of 50–150 mM NaCl to our standard buffer (10 mM piperazine-*N,N'*-bis(2-ethanesulfonic acid), 1 mM Mg, 50 μM GDP or GTP, pH 6.9) enhances overall vinblastine- or vincristine-induced tubulin self-association. As demonstrated in previous studies, GDP enhances overall self-association more than GTP, although in the presence of salt, GDP enhancement is reduced. For example, in 150 mM NaCl, GDP enhancement is 0.24 kcal/mol for vinblastine and 0.36 kcal/mol for vincristine versus an average enhancement of 0.87 ($\pm$ 0.34) kcal/mol for the same drugs in the absence of salt. Wyman linkage analysis of experiments with vinblastine or vincristine over a range of NaCl concentrations showed a twofold increase in the change in NaCl bound to drug-induced spirals in the presence of GTP compared to GDP. These data indicate that GDP enhancement of *Vinca* alkaloid-induced tubulin self-association is due in part to electrostatic inhibition in the GTP state. In the absence of NaCl, we found that vinblastine and 1 mM Mn^{2+} or Ca^{2+} causes immediate condensation of tubulin. The predominant aggregates observed by electron microscopy are large sheets. This effect was not found with 1 mM Mg^{2+}. At 100 μM cation concentrations (Mn^{2+}, Mg^{2+}, or Ca^{2+}), GDP enhances vinblastine-induced spiral formation by 0.55 ($\pm$ 0.26) kcal/mol. This effect is found only in K_2, the association of liganded heterodimers at the ends of growing spirals. There is no GDP enhancement of K_1, the binding of drug to heterodimer, although K_1 is dependent upon the divalent cation concentration. NaCl diminishes tubulin condensation, probably by inhibiting lateral association, and allows an investigation of higher divalent cation concentrations. In the presence of 150 mM NaCl plus 1 mM divalent cations (Mn^{2+}, Mg^{2+}, or Ca^{2+}) GDP enhances vinblastine-induced spiral formation by 0.35 ($\pm$ 0.21) kcal/mol. Relaxation times determined by stopped-flow light scattering experiments in the presence of 150 mM NaCl and vincristine are severalfold longer than those in the presence of vinblastine, consistent with a mechanism involving the redistribution of longer polymers. Unlike previous results in the absence of NaCl, relaxation times in the presence of NaCl are only weakly protein concentration dependent, suggesting the absence of annealing or an additional rate-limiting step in the mechanism.

INTRODUCTION

The antineoplastic *Vinca* alkaloids inhibit microtubule assembly and induce the self-association of tubulin into coiled spiral polymers. We have used sedimentation velocity to determine binding affinities and thermodynamic parameters comparing vincristine-, vinblastine-, and vinorelbine-induced tubulin self-association in 10 mM piperazine-*N,N'*-bis(2-ethanesulfonic acid) (PIPES), pH 6.9, 2 mM EGTA, and 1 mM $MgSO_4$ (Lobert et al., 1995, 1996). The weight-average sedimentation coefficient data are fit with isodesmic ligand-mediated or ligand-mediated plus ligand-facilitated self-association mechanisms (Na and Timasheff, 1985). The presence of GDP significantly enhances spiral formation compared to GTP by about 0.86 ($\pm$ 0.28) kcal/mol, when averaged over all data sets at 25°C for all three drugs. This corresponds to enhancement of the overall process, K_1K_2, where K_1 is the binding of drug to the tubulin heterodimer, and K_2 is liganded-heterodimer binding to a spiral polymer. *Vinca* alkaloids, therefore, can cause disruption of mitotic spindles by first binding to the ends of microtubules, probably as liganded GTP heterodimers, and then inducing spiral propagation into the GDP core of the microtubule. The zipper-like propagation of a spiral into the microtubule lattice that has been observed and described by others (Himes, 1991; Dhamodaran et al., 1995) is thus driven by GDP enhancement of spiral formation.

The interaction of *Vinca* alkaloids with tubulin is known to be strongly dependent upon solution conditions. The wide range (310-fold differences) of apparent binding affinities of vinblastine reported for tubulin are probably due to variations in buffers, ionic strength, and Mg^{2+} concentrations (Himes, 1991; Singer et al., 1988; Na and Timasheff, 1986a,b). Magnesium is known to enhance the assembly of microtubules (Lee and Timasheff, 1977) and the vinblastine-induced self-association of tubulin (Na and Timasheff, 1986b). Interestingly, magnesium also drives the formation of tubulin rings, especially in the presence of GDP (Frigon and Timasheff, 1975a,b; Howard and Timasheff, 1986). The large number of studies summarized by Himes (1991) that report apparent binding affinities, in general, do not properly interpret the interactions in terms of ligand-mediated events (Na and Timasheff, 1985) and thus do not interpret the influence of cations or ionic strength in a quantitative thermodynamic manner. Consequently, there

Received for publication 26 June 1996 and in final form 7 October 1996.
Address reprint requests to Dr. Sharon Lobert, University of Mississippi Medical Center, School of Nursing, 2500 N. State St., Jackson, MS 39216. Tel.: 601-984-6217; Fax: 601-984-1501; E-mail: slobert@fiona.umsmed.edu.

0006-3495/96/01/416/12 $2.00

is a need for a quantitative thermodynamic study of the dependence of *Vinca* alkaloid-induced tubulin self-association on ionic conditions.

Other cations have been reported to interact with tubulin and tubulin polymers. Calcium causes depolymerization of microtubules through interactions with the tubulin carboxyl terminus or with microtubule-associated proteins (MAPs) (Berkowitz and Wolff, 1981; Serrano et al., 1986). Zinc is known to induce sheets of antiparallel protofilaments by binding to an amino-terminal site (Serrano et al., 1988). Manganese will substitute for magnesium, both to induce microtubule assembly and to favor the binding of GTP to the exchangeable nucleotide-binding site (Correia et al., 1988). Cations, especially Mg^{2+} and Ca^{2+}, are also assumed to be important regulators of microtubule assembly in vivo. Furthermore, changes in cell membranes associated with low plasma magnesium levels and mobilization of extracellular and intracellular calcium have been implicated in oncogenesis (reviewed in Kummerow, 1992; Battistini et al., 1993). Hypercalcemia is commonly observed in cancer patients, possibly because of altered humoral factors and/or increased bone resorption (Hoekman and Tjandra, 1991; reviewed in Kaplan, 1994). Thus clinically important changes in intracellular and extracellular calcium or magnesium concentrations may affect the activity of chemotherapeutic agents like *Vinca* alkaloids. We report here the results of sedimentation velocity and stopped-flow, light scattering studies on vinblastine- or vincristine-induced porcine brain tubulin self-association in the presence of NaCl and divalent cations.

MATERIALS AND METHODS

Reagents

Deionized (Nanopure) water was used in all experiments. $ZnSO_4$, $CaSO_4$, $MgSO_4$, EGTA, GDP (Type I), GTP (Type II-S), PIPES, vinblastine sulfate, and vincristine sulfate were purchased from Sigma Chemical Company. $MnSO_4$ was from Fisher Biotech. Sephadex G-50 was from Pharmacia.

Tubulin purification

Porcine brain tubulin (MAP-free phosphocellulose-purified tubulin, PC-tubulin) free of MAPs was obtained by two cycles of warm-cold polymerization-depolymerization followed by phosphocellulose chromatography to separate tubulin from MAPs (Williams and Lee, 1982; Correia et al., 1987). Protein concentrations were determined spectrophotometrically ($\mathscr{E}_{278}$ = 1.2 L/g-cm) (Detrich and Williams, 1978).

Sedimentation velocity experiments

Our methods for sedimentation velocity data collection and analysis have been described previously (Lobert et al., 1995). Sedimentation studies were done in a Beckman Optima XLA analytical ultracentrifuge equipped with absorbance optics and an An60 Ti rotor. Self-association of PC-tubulin (2 μM) in the presence of vinblastine or vincristine and GDP or GTP was investigated. Tubulin samples were equilibrated using spun Sephadex G-50 columns into 10 mM PIPES, pH 6.9, 50 μM GXP, 1 mM $MgSO_4$ in the presence of 50, 100, or 150 mM NaCl. Similar experiments were carried out in the presence of 100 μM $MgSO_4$, $MnSO_4$, or $CaSO_4$ or in the presence of 150 mM NaCl plus 1 mM $MgSO_4$, $MnSO_4$, or $CaSO_4$. The free drug concentration (0.5–70 μM) was obtained from the known drug concentration in the equilibration buffer. After equilibration, the protein was brought to the desired final concentration by dilution with the equilibration buffer. Samples were spun in a Beckman XLA analytical ultracentrifuge at 25°C and appropriate speeds. Temperature was calibrated by the method of Liu and Stafford (1995). Velocity data were collected at 278 nm and at a spacing of 0.01 cm with four averages in a continuous-scan mode. Data was analyzed using software (DCDT) provided by Dr. Walter Stafford (Boston Biomedical Research Institute) to generate a distribution of sedimentation coefficients, $g(s)$, as described previously (Stafford, 1992a,b, 1994; Lobert et al., 1995). The density of each buffer was determined in a Mettler-Paar DMA 02D precision density meter. The viscosity of each buffer was measured in a Cannon-Manning semi-microviscometer.

Curve fitting of sedimentation velocity data

Our method for curve fitting using the ligand-mediated or combined ligand-mediated plus-facilitated models has been described previously (Lobert et al., 1995). In these models, K_1 is the affinity of drug for tubulin heterodimers, K_2 is the affinity of liganded-heterodimers for spiral polymers, K_3 is the affinity of drug for polymers, and K_4 is the association constant for unliganded-tubulin heterodimers. The sedimentation data were plotted as weight-average $\bar{s}_{20,w}$ versus free drug. Total protein concentration in the plateau was determined from $\int g(s)\, ds$. Binding constants were obtained by fitting with the nonlinear least-squares program Fitall (MTR software, Toronto, Canada), modified to include the appropriate fitting functions. Note in this fitting function there are two independent variables, tubulin concentration and drug concentration, and therefore fits are three-dimensional surfaces. The presentation of fits as a two-dimensional figure is typically done at average protein concentrations that do not reflect an accurate goodness of fit.

Reliability of parameters and energetics

In our previous work we discussed the limitations of extracting the four binding parameters implicit in the ligand-mediated and combined models. In the combined model there are only three independent constants, because by microscopic reversibility, $K_1K_2 = K_3K_4$. In previous studies Na and Timasheff (1985, 1986a,b) report that K_4 values of $<1 \times 10^4$ M^{-1} were indistinguishable, and thus in our previous work we fixed $K_4 = 1 \times 10^4$ M^{-1}. This constrained model fit allows for more reproducible parameter estimation. However, in a significant fraction of our previous results (Lobert et al., 1995, 1996) the standard deviations of the constrained and unconstrained fits were identical to or nearly identical to the two parameter ligand-mediated fits. In the current studies we constrain $K_4 = 1 \times 10^3$ M^{-1}, because a number of data sets would not fit with $K_4 = 1 \times 10^4$ M^{-1}. As observed by Na and Timasheff (1985, 1986a,b), this in general has no effect on the quality of the fits and, by the constraint of microscopic reversibility, only affects the magnitude of K_3. The ligand-mediated and the constrained-combined model fits are in general identical, as measured by the standard deviation of the fits (Tables 1 and 3). We continue to report the constrained-combined model fit for comparison with the results of Na and Timasheff (1985, 1986a,b) and our own previous results. We also recognize that thermodynamic exclusion of the facilitated branch is not acceptable and that the binding of the drug to polymer, K_3, is an indicator of linkage and GDP enhancement in the system. Nonetheless, either the data lacks sufficient information to differentiate between the two models or one branch of the thermodynamic loop is kinetically excluded. Note that we previously suggested that the formation of a spiral polymer in the absence of drug, K_4, is probably kinetically excluded, i.e., at these tubulin concentrations, spiral polymers are never observed in the absence of *Vinca* alkaloids. In addition, the spherical approximation used in the fitting function for the sedimentation coefficient of I-mers ($s_i = I^{2/3}s_1$) neglects shape factors, i.e., f/f_0. This is done to compare our results with the

TABLE 1 Equilibrium constants for NaCl effect on *Vinca* alkaloid-induced tubulin association (1 mM Mg^{2+})

[NaCl]	GXP	K_1 (M^{-1})	K_2 (M^{-1})	K_3 (M^{-1})	K_1K_2 (M^{-2})	SD
Vinblastine						
0 mM*	GTP	$1.2 \times 10^5 \pm 0.2$	$5.1 \times 10^6 \pm 0.6$		6.1×10^{11}	0.9
		$1.1 \times 10^5 \pm 0.1$	$7.2 \times 10^4 \pm 1.5$	$8.2 \times 10^6 \pm 0.7$	8.2×10^9	0.9#
	GDP	$1.3 \times 10^5 \pm 0.1$	$2.3 \times 10^7 \pm 0.2$		3.0×10^{12}	0.8
		$1.3 \times 10^5 \pm 1.0$	$1.5 \times 10^5 \pm 1.2$	$1.9 \times 10^7 \pm 0.3$	1.9×10^{10}	0.9#
50 mM	GTP	$1.5 \times 10^5 \pm 0.3$	$6.2 \times 10^6 \pm 0.7$		9.3×10^{11}	1.1
		$1.4 \times 10^5 \pm 0.1$	$7.9 \times 10^4 \pm 0.5$	$1.1 \times 10^7 \pm 0.03$	1.1×10^{10}	1.1#
	GDP	$7.8 \times 10^4 \pm 1.9$	$3.2 \times 10^7 \pm 0.5$		2.5×10^{12}	2.1
		$7.6 \times 10^4 \pm 1.0$	$1.8 \times 10^5 \pm 0.4$	$1.4 \times 10^7 \pm 0.1$	1.4×10^{10}	2.1#
100 mM	GTP	$1.1 \times 10^5 \pm 0.2$	$9.9 \times 10^6 \pm 0.9$		1.1×10^{12}	0.9
		$1.1 \times 10^5 \pm 0.1$	$1.0 \times 10^5 \pm 0.1$	$1.1 \times 10^7 \pm 0.1$	1.1×10^{10}	0.9#
	GDP	$1.2 \times 10^5 \pm 0.2$	$2.8 \times 10^7 \pm 0.2$		3.4×10^{12}	1.3
		$1.2 \times 10^5 \pm 0.03$	$1.7 \times 10^5 \pm 0.1$	$2.0 \times 10^7 \pm 0.04$	2.0×10^{10}	1.3#
150 mM	GTP	$1.2 \times 10^5 \pm 0.3$	$1.3 \times 10^7 \pm 0.1$		1.6×10^{12}	1.7
		$1.2 \times 10^5 \pm 0.1$	$1.1 \times 10^5 \pm 2.0$	$1.4 \times 10^7 \pm 0.1$	1.4×10^{10}	1.7#
	GDP	$9.1 \times 10^4 \pm 1.6$	$3.4 \times 10^7 \pm 0.4$		3.1×10^{12}	1.5
		$8.9 \times 10^4 \pm 0.8$	$1.8 \times 10^5 \pm 0.3$	$1.6 \times 10^7 \pm 0.1$	1.6×10^{10}	1.6#
Vincristine						
0 mM§	GTP	$1.4 \times 10^5 \pm 0.4$	$1.7 \times 10^7 \pm 0.4$		2.3×10^{12}	1.2
		$1.3 \times 10^5 \pm 0.05$	$1.3 \times 10^5 \pm 0.1$	$1.7 \times 10^7 \pm 0.1$	1.7×10^{10}	1.2#
	GDP	$2.1 \times 10^5 \pm 0.4$	$3.9 \times 10^7 \pm 0.5$		7.9×10^{12}	1.7
		$2.0 \times 10^5 \pm 0.2$	$1.9 \times 10^5 \pm 0.4$	$4.0 \times 10^7 \pm 0.3$	4.0×10^{10}	1.7#
50 mM	GTP	$1.3 \times 10^5 \pm 0.2$	$3.2 \times 10^7 \pm 0.3$		4.3×10^{12}	1.5
		$1.3 \times 10^5 \pm 0.1$	$1.8 \times 10^5 \pm 0.3$	$2.3 \times 10^7 \pm 0.2$	2.3×10^{10}	1.6#
	GDP	$2.1 \times 10^5 \pm 0.2$	$6.4 \times 10^7 \pm 0.3$		1.3×10^{13}	1.3
		$2.0 \times 10^5 \pm 0.9$	$2.6 \times 10^5 \pm 1.2$	$5.2 \times 10^7 \pm 0.2$	5.2×10^{10}	1.3#
100 mM	GTP	$1.7 \times 10^5 \pm 0.3$	$4.3 \times 10^7 \pm 0.4$		7.2×10^{12}	1.7
		$1.6 \times 10^5 \pm 0.1$	$2.1 \times 10^5 \pm 0.3$	$3.3 \times 10^7 \pm 0.2$	2.3×10^{10}	1.8#
	GDP	$1.6 \times 10^5 \pm 0.2$	$9.6 \times 10^7 \pm 0.7$		1.5×10^{13}	1.9
		$1.6 \times 10^5 \pm 0.1$	$3.1 \times 10^5 \pm 0.4$	$4.9 \times 10^7 \pm 0.3$	4.9×10^{10}	2.0#
150 mM	GTP	$1.4 \times 10^5 \pm 0.3$	$4.7 \times 10^7 \pm 0.5$		6.7×10^{12}	2.0
		$1.4 \times 10^5 \pm 0.4$	$2.2 \times 10^5 \pm 0.6$	$3.0 \times 10^7 \pm 0.1$	3.0×10^{10}	2.0#
	GDP	$1.7 \times 10^5 \pm 0.3$	$8.3 \times 10^7 \pm 0.6$		1.4×10^{13}	2.0
		$1.7 \times 10^5 \pm 0.1$	$2.9 \times 10^5 \pm 0.4$	$4.9 \times 10^7 \pm 0.3$	4.9×10^{10}	2.0#

*0 mM NaCl data with vinblastine from Lobert et al. (1995) shown here for clarity of presentation.
#K_4 constrained at 10^3 M^{-1}.
§0 mM NaCl data with vincristine from Lobert et al. (1996) shown here for clarity of presentation.

previous and extensive work of Timasheff and co-workers (Na and Timasheff, 1986a,b), who used the same model. Also, as previously reported (Lobert et al., 1995), fits including f/f_0 did not improve the variance of the fit, although the overall affinity increases. We anticipate that future experiments at higher divalent cation concentrations may force us to distinguish between single and double filament spirals, possibly by the inclusion of distinct shape factors. Thus we continue to favor the ligand-mediated fits as the best quantitative indicators of overall association for the following reasons: 1) the standard deviations of these fits are equivalent to or better than those from the combined model; 2) at 2 μM tubulin, the contribution of K_4 to the overall energetics is probably not significant; and 3) the ligand-mediated fits are most likely better estimates of the total energetics of the process.

Wyman linkage analysis of NaCl and divalent cation dependence

The linkage of NaCl or divalent cation binding to *Vinca* alkaloid-induced tubulin self-association was analyzed using Wyman linkage theory (Wyman, 1964). It is based upon the thermodynamic principle that a change in the activity of any species affects the activity of all other species in solution. The Wyman linkage relationship is

$$(\delta \ln K/\delta \ln a_3)_{T,P,m2} = \Delta\nu,$$

where K is the equilibrium constant for the reaction at constant temperature, pressure, and protein concentration; a_3 is the activity of ligand; and $\Delta\nu$ is the change in apparent additional binding of component 3 to the protein, component 2, during the reaction. Note that it reflects a change in binding and not total amount bound, and is thus referred to as preferential interaction (Wyman, 1964; Lee and Timasheff, 1977; Correia, 1991). Sedimentation velocity data were collected at 25°C in the presence of GXP over a range of NaCl concentrations (0–150 mM NaCl), and binding parameters were determined as described above. Data collected in these studies and in prior studies at various divalent cation concentrations were also compared (Prakash and Timasheff, 1985; Na and Timasheff, 1986a,b; Lobert et al., 1995, 1996).

Stopped-flow light scattering experiments

Our procedure for manual stopped-flow light scattering experiments (Hi-Tech manual stopped-flow apparatus) has been described previously (Lobert et al., 1996). After equilibrating PC-tubulin (0.2–3 μM) solutions into 10 mM PIPES, pH 6.9, 150 mM NaCl, 2 mM EGTA, 1 mM $MgSO_4$, 50 μM GTP, and 50 μM vinblastine or vincristine, samples were degassed for 1 h at room temperature. Experiments were initiated by rapid mixing (deadtime < 1 s) of tubulin samples 1:1 with the same buffer without drug and then monitoring with a SLM Aminco Bowman Series 2 luminescence spectrometer over 10 min at 1-s intervals. The final drug and tubulin

concentrations were 25 or 12.5 μM and 0.1–1.5 μM, respectively. Data were fit and analyzed as described by Lobert et al. (1996).

Electron microscopy

Tubulin samples were prepared at room temperature in the presence of 50 μM vincristine or vinblastine in 10 mM PIPES, pH 6.9, 50 μM GXP, and 100 μM or 1 mM $MgSO_4$, $MnSO_4$, or $CaSO_4$. The method used for glutaraldehyde fixation and negative staining with uranyl acetate has been described previously (Lobert et al., 1995).

RESULTS

Ionic strength effects

To determine the effect of ionic strength on *Vinca* alkaloid-induced tubulin association, we carried out sedimentation velocity studies at 25°C in the presence of vinblastine, 1 mM $MgSO_4$, and 50, 100, or 150 mM NaCl. Fig. 1 shows $\bar{s}_{20,w}$ values, calculated from these data, plotted versus free vinblastine concentrations in the presence of NaCl and GDP or GTP. Binding affinities obtained from fits of these data with the ligand-mediated or ligand-mediated-plus facilitated models are given in Table 1. Binding parameters determined in the absence of NaCl, reported previously (Lobert et al., 1995), are included for clarity of presentation. When data collected in the presence of GTP are fit with the ligand-mediated model, the overall binding affinities, K_1K_2, increase with increasing NaCl concentrations, with values ranging from 6.1×10^{11} M^{-2} in the absence of NaCl to 1.6×10^{12} M^{-2} in 150 mM NaCl. Over the same NaCl concentrations, in the presence of GDP, K_1K_2 does not change significantly, ranging from 2.5×10^{12} M^{-2} to 3.1×10^{12} M^{-2}, with a mean value of $3.1 (\pm 0.37) \times 10^{12}$ M^{-2}. Similar trends are obtained with the combined ligand-mediated-plus facilitated model. Thus NaCl enhances vinblastine-induced spiral formation more dramatically in the presence of GTP than in the presence of GDP, and the GDP enhancement of tubulin spiral formation previously reported for vinblastine (Lobert et al., 1995) is significantly reduced at higher salt concentrations. For example, at 25°C in 150 mM NaCl, the GDP enhancement from a mediated fit is 0.39 kcal/mol versus 0.94 kcal/mol in the absence of NaCl (Lobert et al., 1995). In 150 mM NaCl the average GDP enhancement for both models is 0.24 ± 0.22 kcal/mol compared to 0.75 ± 0.28 kcal/mol in the absence of NaCl (Lobert et al., 1996). Wyman linkage analysis (Wyman, 1964) of NaCl concentration and overall binding affinity, K_1K_2, demonstrated that the change in NaCl binding to vinblastine-induced spirals is increased twofold in the presence of GTP compared to GDP. For example, when data collected in the presence of GTP are fit with the ligand-mediated model, each mole of tubulin binds an additional 0.464 (± 0.175) mole of NaCl. In the presence of GDP only an additional 0.227 (± 0.176) mol/mol binds. Because NaCl enhances assembly in the presence of GTP more than in the presence of GDP, it appears that about 50% of the GDP enhancement is due to an electrostatic inhibition in the GTP state.

We have recently demonstrated that GDP enhancement of spiral formation is also exhibited by vincristine and vinorelbine (Lobert et al., 1996). To determine whether the NaCl effects observed with vinblastine may be characteristic of other *Vinca* alkaloids, we carried out similar sedimentation experiments with vincristine in the presence of 1 mM $MgSO_4$ and 50, 100, or 150 mM NaCl. Fig. 2 shows $\bar{s}_{20,w}$ values plotted versus free vincristine concentrations in the presence of NaCl and GDP or GTP at 25°C. Table 1 gives

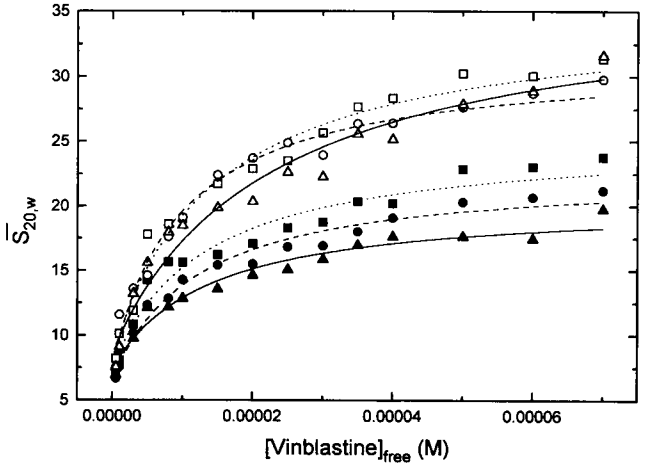

FIGURE 1 Plots of $\bar{s}_{20,w}$ values versus free vinblastine concentrations at 25°C. Initial tubulin in all experiments was 2 μM in the presence of 50 μM GDP (*open symbols*) or GTP (*closed symbols*). The buffers were 10 mM PIPES, pH 6.9, 1 mM $MgSO_4$, 50 μM GXP, and NaCl concentrations at 50 mM (▲, △), 100 mM (●, ○), or 150 mM (■, □). The lines represent fits using the ligand-mediated model for 50 (——), 100 (– – –), or 150 (·····) mM NaCl.

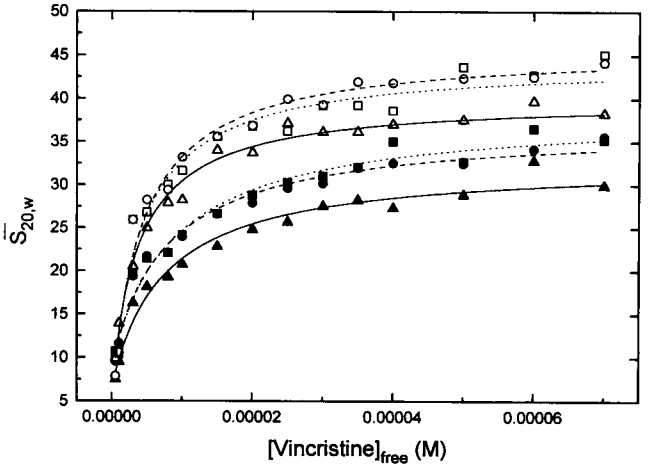

FIGURE 2 Plots of $\bar{s}_{20,w}$ values versus free vincristine concentrations at 25°C. Initial tubulin in all experiments was 2 μM in the presence of 50 μM GDP (*open symbols*) or GTP (*closed symbols*). The buffers were 10 mM PIPES, pH 6.9, 1 mM $MgSO_4$, 50 μM GXP, and NaCl concentrations at 50 mM (▲, △), 100 mM (●, ○), or 150 mM (■, □). The lines represent fits using the ligand-mediated model for 50 (——), 100 (– – –), or 150 (·····) mM NaCl.

the binding parameters obtained from fits of these data. Data collected in the absence of NaCl (Lobert et al., 1996) are included for clarity. In the presence of vincristine, as with vinblastine, NaCl enhances self-association more dramatically in the presence of GTP than with GDP. The overall affinity K_1K_2 (derived from ligand-mediated fits) is increased approximately threefold in the presence of GTP versus 1.9-fold in the presence of GDP. At 25°C in 150 mM NaCl, the GDP enhancement with vincristine from a ligand-mediated fit is reduced to 0.44 kcal/mol versus 0.73 kcal/mol in the absence of NaCl (Lobert et al., 1996). Wyman linkage analysis of the overall affinity, K_1K_2, derived from ligand-mediated fits versus NaCl concentration, demonstrated that vincristine-induced tubulin spirals also bind less NaCl in the presence of GDP compared to GTP. Each mole of tubulin binds an additional 0.438 (± 0.249) and 0.079 (± 0.098) mole of NaCl for GTP and GDP conditions. Thus it appears that approximately half of the GDP enhancement for both vinblastine- and vincristine-induced self-association of tubulin is due to an electrostatic inhibition in the GTP state that can be partially overcome by NaCl. This is most likely due to a conformation in GTP-tubulin that causes or induces repulsive interactions in a spiral polymer.

Kinetics of *Vinca* alkaloid-induced tubulin self-association

To further investigate the importance of ionic strength in the mechanism of *Vinca* alkaloid-induced spiral formation, we carried out stopped-flow light scattering experiments in the presence of 150 mM NaCl over a range of tubulin concentrations with vinblastine or vincristine. We had shown previously that in the absence of NaCl, vincristine relaxation times are more than 20-fold longer than those in the presence of vinblastine (Lobert et al., 1996). Additionally for vinblastine (and vinorelbine), we found a protein concentration dependence, where increasing protein concentration resulted in decreasing relaxation times. These data indicated that vinblastine-induced spiral formation occurs by the addition of oligomers, as well as heterodimers to the ends of polymers (Thusius et al., 1975). Annealing of oligomers to the ends of vinblastine-induced spirals has been suggested previously by the results of x-ray scattering studies (Hodgkinson et al., 1992; Nogales et al., 1995a). This concentration dependence was not observed with vincristine, probably because of the fact that the vincristine data were fit best with two exponentials, suggesting two or more steps in the relaxation process, and thus causing an additional propagation of error in the first relaxation time. We suggested that the additional steps involved the alignment of spirals. In the experiments here at room temperature with 150 mM NaCl, the initial drug concentrations were 50 or 25 μM, and initial protein concentrations ranged from 0.2 to 3.0 μM. The light scattering experiments were initiated by diluting the drug and protein to half the starting concentration. Typical relaxation experiments for vinblastine and vincristine are shown in Fig. 3. Relaxation times determined from an average of three or more experiments are given in Table 2. In the experiments shown here in the presence of NaCl, both the vinblastine and vincristine data were fit best with a single exponential. The relaxation times in the presence of vinblastine and 150 mM NaCl were similar to those found in the absence of NaCl (Lobert et al., 1996). The relaxation times in the presence of vincristine and 150 mM NaCl are more than threefold longer than those found in the presence of vinblastine, consistent with the formation of longer spirals with vincristine. These relaxation times are similar to the τ_1 values previously observed for vincristine-induced spirals (Lobert et al., 1996) and are assigned to the dissociation of heterodimers or oligomers from the spiral polymers. The second relaxation time τ_2 previously observed with vincristine is completely missing in 150 mM NaCl. Thus high NaCl concentration suppresses the alignment of vincristine-induced spirals, probably by diminishing lateral interactions between spirals.

The vinblastine data demonstrate decreasing relaxation times with increasing protein concentration (Table 2), similar to the results found in the absence of NaCl (Lobert et al., 1996). A plot of $1/\tau^2$ versus the final protein concentration can be used to estimate k_{on} and k_{off} values, as described previously (Thusius et al., 1975; Lobert et al., 1996). However, the association constant, K, estimated from k_{on} and k_{off}, is smaller than K_2 (Table 1) by more than an order of magnitude, 1.0×10^6 M^{-1} and 4.7×10^7 M^{-1}, respectively. This kinetically determined association constant, K, is also smaller than $K_{2,app}$ (Na and Timasheff, 1985), the drug-dependent apparent association constant

$$K_{2,app} = K_2/[1 + 1/(K_1[X])]^2$$

(where X is the free drug concentration), found here to be equal to 7.3–9.6 $\times$ 10^6 M^{-1} at 25–50 μM free drug con-

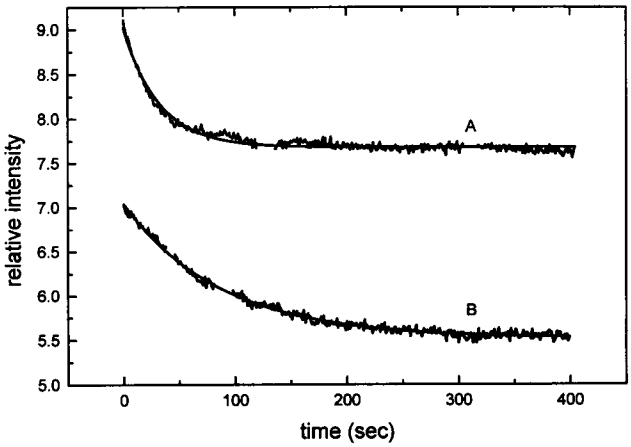

FIGURE 3 Stopped-flow, light-scattering experiments. Relative intensity is plotted versus time (s). As described in Materials and Methods, the drug concentrations were initially 50 μM. The buffers were 10 mM PIPES, pH 6.9, 1 mM $MgSO_4$, 2 mM EGTA, 50 μM GTP, and 150 mM NaCl. Following dilution to 25 μM drug, scattering was monitored over 10 min at 1-s intervals. *Upper curve*: Vinblastine. *Lower curve*: Vincristine.

TABLE 2 Stopped-flow light scattering

Drug	[Tubulin] μM (initial)	A1	τ (s)
Vinblastine	0.4	0.82 ± 0.01	44.56 ± 31.56
	0.5	0.98 ± 0.11	33.34 ± 4.73
	0.8	0.68 ± 0.04	29.82 ± 3.30
	1.0	0.96 ± 0.37	26.21 ± 1.12
	1.3	1.08 ± 0.06	25.38 ± 1.70
Vincristine	0.2	0.34 ± 0.07	105.66 ± 30.54
	0.5	0.73 ± 0.10	117.15 ± 20.43
	0.7	0.99 ± 0.05	100.85 ± 3.96
	0.8	1.22 ± 0.01	97.19 ± 7.08
	1.2	1.21 ± 0.15	99.13 ± 2.83

Drug dilution, 25–12.5 μM; 10 mM PIPES, pH 6.9, 150 mM NaCl, 2 mM EGTA, 1 mM $MgSO_4$, 50 μM GTP.

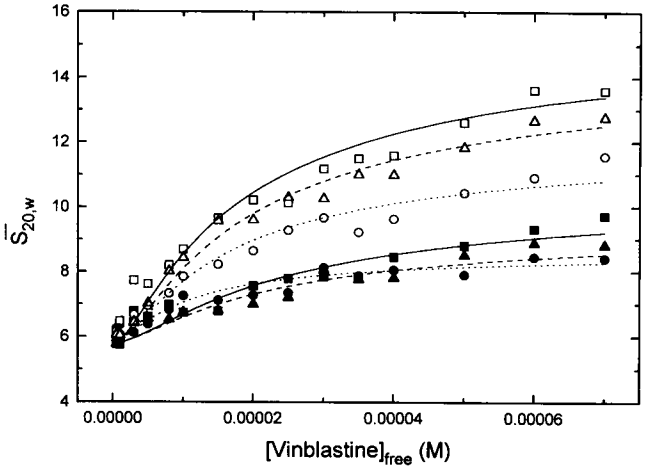

FIGURE 4 Plots of $\bar{s}_{20,w}$ values versus free vinblastine concentrations at 25°C. Tubulin in all experiments was 2 μM in the presence of 50 μM GDP (*open symbols*) or GTP (*closed symbols*). The buffers were 10 mM PIPES, pH 6.9, 50 μM GXP, and 100 μM Mn^{2+} (■, □), Ca^{2+} (●, ○), or Mg^{2+} (▲, △). The lines represent fits using the ligand-mediated model for Mn^{2+} (——),Mg^{2+} (– – –), or Ca^{2+} (·····).

centrations. Thus this 7–15-fold difference suggests that in high salt the model previously used to interpret these data (Thusius et al., 1975) is not applicable. Furthermore, vincristine relaxation times have an extremely weak concentration dependence that precludes the estimation of k_{on} and k_{off}. Either annealing is not occurring in high salt or additional steps complicate its determination. For example, in high salt k_{on} or k_{off} may be tightly coupled to a conformational change, salt release, and/or drug binding to the polymer.

Divalent cation effects

We performed initial experiments on the influence of other divalent cations on vinblastine-induced tubulin self-association. However, we found that in a low ionic strength buffer with 1 mM Zn^{2+}, Mn^{2+}, or Ca^{2+}, vinblastine caused condensation of tubulin. The primary aggregates observed by electron microscopy were large amorphous sheets (data not shown). (This is consistent with the previous report by Na and Timasheff (1986b) that in >2.5 mM Mg^{2+} and low ionic strength buffer large aggregates are formed. It is also consistent with earlier electron microscopy and turbidity studies demonstrating that >8 mM Ca^{2+} induced extensive aggregation of *Vinca* alkaloid-induced tubulin spirals (Wilson et al., 1970; Himes et al., 1976).) Sedimentation velocity experiments could be performed at lower divalent cation concentrations, although 100 μM Zn^{2+} still caused condensation and was not pursued in further studies. Fig. 4 is a plot of free vinblastine concentrations versus $\bar{s}_{20,w}$ values calculated for sedimentation data collected at 25°C in the presence of 100 μM Mg^{2+}, Mn^{2+}, or Ca^{2+} and GDP or GTP. There are two things to be noted about these data. First, it can be seen that for all three cations, GDP enhances spiral formation compared to GTP. The largest enhancement is with Mn^{2+} and the smallest enhancement is with Ca^{2+}. Second, the effect of changing the divalent cation in these solutions occurs primarily in the GDP samples and not in the GTP samples. Binding affinities obtained from fits of these data with ligand-mediated or ligand-mediated-plus facilitated models are given in Table 3. With the exception of the Ca^{2+} data, there is no GDP effect on K_1, the affinity of vinblastine for the tubulin heterodimer. The enhancement resides entirely in K_2, the affinity of liganded-heterodimers for spirals, and K_3, the affinity of the drug for polymers. The overall enhancement in K_1K_2, derived from ligand-mediated fits, is 0.83 kcal/mol for Mn^{2+}, 0.80 kcal/mol for Mg^{2+}, and 0.24 kcal/mol for Ca^{2+}. This suggests a differential effect of divalent cations on spiral formation. The mean overall GDP enhancement for 100 μM Mn^{2+} and Mg^{2+} data fit with both the ligand-mediated model and the ligand-mediated-plus facilitated model equals 0.63 (± 0.22) kcal/mol. This is less than the 0.86 kcal/mol enhancement observed with 1 mM Mg^{2+} and thus is consistent with a general divalent cation effect on spiral formation (Himes, 1991; Na and Timasheff, 1986b).

The average K_1 from these experiments for Mn^{2+} and Mg^{2+} conditions is 5.0 (± 0.5) × 10^4 M^{-1}, in good agreement with the results of Na and Timasheff (1986a) for vinblastine in the absence of Mg^{2+} (3.8 × 10^4 M^{-1}), but under weaker ionic conditions (10 mM phosphate, pH 7.0, and 0.1 mM GTP). In fact, Prakash and Timasheff (1985) observed a similar K_1 value for vincristine (3.5 × 10^4 M^{-1}) in the absence of Mg^{2+}. Consistent with our previous observation (Lobert et al., 1996), K_1 is not dependent upon the *Vinca* alkaloid, but it does appear to depend upon the divalent cation concentration. In 1 mM Mg^{2+} in the absence of salt at 25°C, we observed an average K_1 value of 1.55 (± 0.34) × 10^5 M^{-1} for vinblastine, vincristine, and vinorelbine (Lobert et al., 1996). Thus K_1 increases with Mg^{2+} concentration.

In the presence of 100 μM Ca^{2+} and GTP, we found K_1 to be nearly threefold larger, 1.3 (± 0.1) × 10^5 M^{-1}, than in the presence of 100 μM Mn^{2+} or Mg^{2+}. In the presence

TABLE 3 Equilibrium constants for cation effect on vinblastine-induced tubulin association

Cation	GXP	K_1 (M^{-1})	K_2 (M^{-1})	K_3 (M^{-1})	K_1K_2 (M^{-2})	SD
100 μM divalent cation						
Mn^{2+}	GTP	$4.8 \times 10^4 \pm 1.3$	$1.0 \times 10^6 \pm 2.1$		4.7×10^{10}	0.4
		$4.1 \times 10^4 \pm 0.5$	$3.3 \times 10^4 \pm 0.7$	$1.3 \times 10^6 \pm 0.1$	1.3×10^9	0.4*
	GDP	$5.3 \times 10^4 \pm 1.1$	$3.5 \times 10^6 \pm 0.5$		1.9×10^{11}	0.6
		$4.9 \times 10^4 \pm 0.5$	$6.0 \times 10^4 \pm 1.2$	$2.9 \times 10^6 \pm 0.2$	2.9×10^9	0.6
Mg^{2+}	GTP	$5.9 \times 10^4 \pm 1.6$	$6.6 \times 10^5 \pm 1.1$		3.9×10^{10}	0.3
		$5.0 \times 10^4 \pm 0.2$	$2.7 \times 10^4 \pm 0.2$	$1.3 \times 10^6 \pm 0.03$	1.3×10^9	0.3*
	GDP	$5.2 \times 10^4 \pm 0.8$	$2.9 \times 10^6 \pm 0.3$		1.5×10^{11}	0.4
		$4.7 \times 10^4 \pm 0.3$	$5.4 \times 10^4 \pm 0.8$	$2.6 \times 10^6 \pm 0.1$	2.6×10^9	0.4*
Ca^{2+}	GTP	$1.4 \times 10^5 \pm 0.5$	$4.7 \times 10^5 \pm 0.7$		6.7×10^{10}	0.4
		$1.2 \times 10^5 \pm 0.1$	$2.2 \times 10^4 \pm 0.5$	$2.7 \times 10^6 \pm 0.3$	2.7×10^9	0.4*
	GDP	$6.9 \times 10^4 \pm 1.0$	$1.5 \times 10^6 \pm 0.1$		1.0×10^{11}	0.3
		$6.3 \times 10^4 \pm 0.4$	$3.9 \times 10^4 \pm 1.2$	$2.5 \times 10^6 \pm 0.1$	2.5×10^9	0.3*
150 mM NaCl, 1 mM divalent cation						
Mn^{2+}	GTP	$9.8 \times 10^4 \pm 2.2$	$1.6 \times 10^7 \pm 0.2$		1.5×10^{12}	1.5
		$9.4 \times 10^4 \pm 1.1$	$1.3 \times 10^5 \pm 0.3$	$1.2 \times 10^7 \pm 0.1$	1.2×10^{10}	1.6*
	GDP	$1.3 \times 10^5 \pm 0.2$	$3.5 \times 10^7 \pm 0.2$		4.6×10^{12}	1.1
		$1.3 \times 10^5 \pm 0.1$	$1.9 \times 10^5 \pm 0.2$	$2.4 \times 10^7 \pm 0.1$	2.4×10^{10}	1.2*
Mg^{2+}	GTP	$1.2 \times 10^5 \pm 0.3$	$1.3 \times 10^7 \pm 0.1$		1.6×10^{12}	1.3
		$1.2 \times 10^5 \pm 0.1$	$1.1 \times 10^5 \pm 0.2$	$1.4 \times 10^7 \pm 0.1$	1.4×10^{10}	1.3*
	GDP	$9.1 \times 10^4 \pm 1.6$	$3.4 \times 10^7 \pm 0.4$		3.1×10^{12}	1.5
		$8.9 \times 10^4 \pm 0.8$	$1.8 \times 10^5 \pm 0.3$	$1.6 \times 10^7 \pm 0.1$	1.6×10^{10}	1.6*
Ca^{2+}	GTP	$1.4 \times 10^5 \pm 0.2$	$1.2 \times 10^7 \pm 0.1$		1.7×10^{12}	1.0
		$1.4 \times 10^5 \pm 0.1$	$1.1 \times 10^5 \pm 0.2$	$1.5 \times 10^7 \pm 0.1$	1.5×10^{10}	1.1*
	GDP	$1.3 \times 10^5 \pm 0.3$	$2.5 \times 10^7 \pm 0.3$		3.3×10^{12}	1.6
		$1.3 \times 10^5 \pm 0.04$	$1.6 \times 10^5 \pm 0.05$	$2.0 \times 10^7 \pm 0.1$	2.0×10^{10}	1.6*

*K_4 constrained at 10^3 M^{-1}.

of Ca^{2+} and GDP, K_1 is more similar to, although still larger than, its value in the presence of Mg^{2+} and Mn^{2+}. It is not clear whether this observation is a fitting artifact or is indicative of a real trend in the data (see below). Note that the data collected in the presence of Ca^{2+} and fit with the combined model do not demonstrate an overall GDP enhancement. This is due to the fact that although K_2 is larger when GDP is present, K_1 is smaller and thus the overall effect in K_1K_2 shows no enhancement by GDP. Additionally, for this combined fit there is no enhancement in K_3. Clearly, however, from the plot of $\bar{s}_{20,w}$ versus free vinblastine concentrations (Fig. 4), GDP does enhance the polymer size distribution in the presence of Ca^{2+}. This GDP enhancement under Ca^{2+} conditions is best represented by the overall mediated fit, corresponding to 0.24 kcal/mol, or by K_2 alone in the mediated or combined fits, corresponding to 0.69 and 0.34 kcal/mol, respectively.

To work at high divalent cation concentrations, we explored the influence of NaCl on tubulin condensation. NaCl suppresses divalent cation-induced tubulin condensation, and thus in the presence of 150 mM NaCl we were able to carry out studies of cation effects at 1 mM concentrations by sedimentation velocity. Note that this observation is consistent with the earlier work by Himes et al. (1976) and the subsequent work by Na and Timasheff (1986b) that showed NaCl suppressed the formation of larger aggregates in the presence of *Vinca* alkaloids. Fig. 5 is a plot of free vinblastine concentrations versus $\bar{s}_{20,w}$ values calculated from data collected at 25°C in the presence of vinblastine, 150 mM NaCl, and 1 mM Mg^{2+}, Mn^{2+}, or Ca^{2+} and GDP or GTP. The data are similar to the 100 μM divalent cation data (Fig. 4) in that 1) there is a GDP enhancement for all three conditions, and 2) the primary difference between the cations is in the GDP data sets, not the GTP data sets. Table 3 gives the binding parameters obtained from fits of the data.

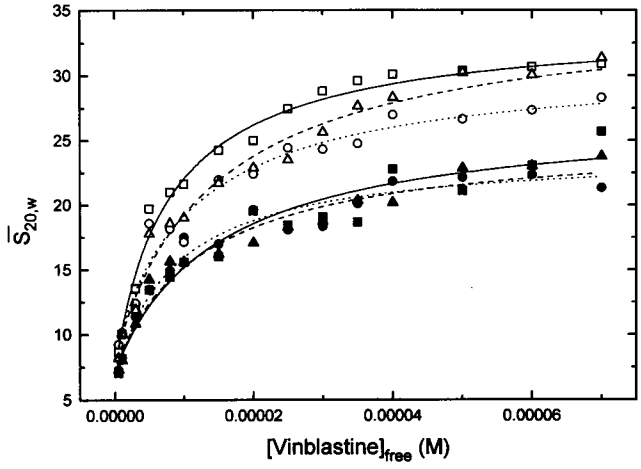

FIGURE 5 Plots of $\bar{s}_{20,w}$ values versus free vinblastine concentrations at 25°C. Tubulin in all experiments was 2 μM in the presence of 50 μM GDP (*open symbols*) or GTP (*closed symbols*). The buffers were 10 mM PIPES, pH 6.9, 50 μM GXP, 150 mM NaCl, and 1 mM Mn^{2+} (■, □), Ca^{2+} (●, ○), or Mg^{2+} (▲, △). The lines represent fits using the ligand-mediated model for Mn^{2+} (——), Mg^{2+} (– – –), or Ca^{2+} (·····).

Regardless of the parameters chosen to compare between the 100 μM and 1 mM Mg^{2+} and Mn^{2+} data, these results represent a suppression of the $\Delta\Delta G$ for GDP enhancement by the presence of 150 mM NaCl. This is in complete agreement with the NaCl titration data presented in Figs. 1 and 2 and Table 1.

Examination of the divalent cation data reveals that there is no significant difference among the three cations in overall binding affinity in the presence of GTP. For example, when data are fit with the ligand-mediated model for all three cations, the mean overall binding affinity, K_1K_2, in the presence of GTP is 1.6 ($\pm$ 0.1) $\times$ 10^{12} M^{-2}. In the presence of GDP there are small divalent cation-dependent trends in the data. For the overall binding affinity, K_1K_2, Mn^{2+} gives the largest ligand-mediated value (4.6 $\times$ 10^{12} M^{-2}), whereas the Ca^{2+} and Mg^{2+} data give similar values (3.3 versus 3.1 $\times$ 10^{12} M^{-2}). This corresponds to GDP enhancements of 0.66, 0.39, and 0.39 kcal/mol for Mn^{2+}, Ca^{2+}, and Mg^{2+} conditions, respectively. However, in terms of K_2, the binding of liganded heterodimer to spirals, Mn^{2+} and Mg^{2+} give similar values (3.5 and 3.4 $\times$ 10^7 M^{-1}), whereas Ca^{2+} gives a smaller value (2.5 $\times$ 10^7 M^{-1}). This corresponds to GDP enhancements of 0.46, 0.45, and 0.56 kcal/mol for Mn^{2+}, Ca^{2+}, and Mg^{2+} conditions, respectively. Similar trends are found with the combined model. The small variations observed with 100 μM and 1 mM Ca^{2+} may be due to propagation of error in the fitting. However, the trends in the primary data, especially in the presence of GDP, clearly show smaller maximum $\bar{s}_{20,w}$ values for Ca^{2+} compared to the other two cations (Fig. 5). To investigate these data further, we carried out simulations of ligand-mediated and ligand-mediated-plus facilitated association (Fig. 6), varying K_1 or K_2. For the ligand-mediated model simulations in Fig. 6 *B*, K_1 is fixed at an average experimental value of 1.2 $\times$ 10^5 M^{-1}, and K_2 is varied from 1 to 4 $\times$ 10^7 M^{-1}. For the combined model simulations in Fig. 6 *A*, K_1 and K_4 are fixed and K_3 is increased from 5 $\times$ 10^6 to 3 $\times$ 10^7 M^{-1}. K_2 necessarily also increases to maintain microscopic reversibility. The 1 mM Ca^{2+} and Mn^{2+} data in the presence of GDP (Table 3) are plotted on the figures for comparison. In addition, to explore the role of K_1 on the shapes of the curves, a ligand-mediated simulation (Fig. 6 *C*) with fixed K_2 and variable K_1 was performed. The 100 μM Ca^{2+} and Mn^{2+} data in the presence of GTP (Table 3) are plotted on the figures for comparison. At fixed K_1 values, it is clear that the plateau value determines the magnitude of K_2 for both the ligand-mediated and the combined models (Fig. 6, *A* and *B*). Thus the smaller K_2 values for the Ca^{2+} data are due to a lower maximum $\bar{s}_{20,w}$ value, indicating that in the presence of Ca^{2+}, vinblastine does induce smaller polymers than in the presence of the other cations. The simulation at fixed K_2 (Fig. 6 *C*) shows that as K_1 increases, the steepness of the curve at low vinblastine concentrations increases. Furthermore, because K_1K_2 increases, the plateau values increase, indicating that an increase in liganded heterodimer concentration (due to increasing K_1) provides more drug-tubulin complexes for self-association at a fixed K_2. From

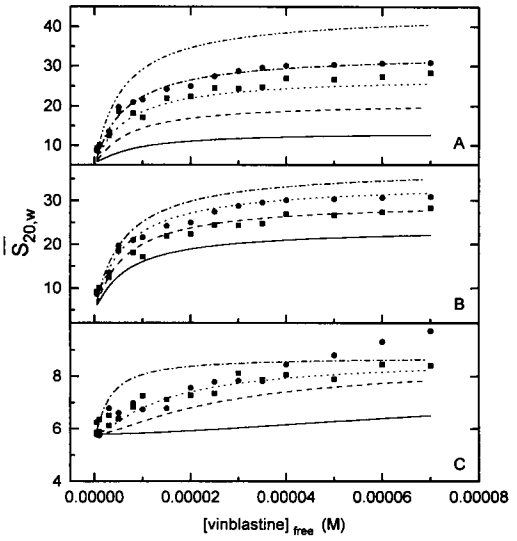

FIGURE 6 Plots of simulations of $\bar{s}_{20,w}$ values versus free vinblastine concentrations at 25°C. (*A*) Ligand-mediated plus-facilitated model simulations at fixed K_1, 1.2 $\times$ 10^5 M^{-1}, fixed K_4, 1.0 $\times$ 10^3 M^{-1}, and variable K_3 of 0.5 (——), 1.0 (– – –), 1.5 (·····), 2.0 (–·–), and 3.0 (–··–) $\times$ 10^7 M^{-1}. (*B*) Ligand-mediated simulations at fixed K_1, 1.2 $\times$ 10^5 M^{-1}, and variable K_2 of 1.0 (——), 2.0 (– – –), 3.0 (·····), and 4.0 (–·–) $\times$ 10^7 M^{-1}. Data points from sedimentation velocity experiments at 1 mM Mn^{2+} (●) and 1 mM Ca^{2+} (■) are overlaid. (*C*) Ligand-mediated simulations at fixed K_2, 4.7 $\times$ 10^5 M^{-1}, and variable K_1 of 0.1 (——), 0.5 (– – –), 1.0 (·····), and 5.0 (–·–) $\times$ 10^5 M^{-1}. Data points from sedimentation velocity experiments at 100 μM Mn^{2+} (●) and 100 μM Ca^{2+} (■) are overlaid.

the perspective of fitting these data, at a given plateau value, K_1 is determined by the steepness of the curve at low drug concentrations. In the case of 100 μM Ca^{2+} (see Fig. 6 *C*), the lowest drug concentration points, at 0.5 and 1 μM, are significantly above the heterodimer value of 5.8 S. Thus these points appear to dictate the larger K_1 observed in the Ca^{2+}, GTP fits (Table 3). Realizing the significance of these low drug concentration data points, we gathered an additional set of data at 0.5, 1, and 3 μM vinblastine and 100 μM Ca^{2+}. All six data points are shown in Fig. 6 *C* and are used to determine the K_1 value reported in Table 3. Although the magnitude of the repeated $\bar{s}_{20,w}$ values at low drug concentrations were significantly lower by about 6% at each point, the values for K_1 (Table 3) remain higher than those for data collected in the presence of Mn^{2+} or Mg^{2+}. Fits that excluded the original three points gave K_1 values only slightly smaller, 1.1 $\times$ 10^5 M^{-1}. This confirms the conclusions derived from the simulations, that the initial slope relative to the plateau concentration dictates the magnitude of K_1. In this case the lower plateau with the Ca^{2+} data forces a larger K_1 value relative to the Mn^{2+} or Mg^{2+} data.

Finally, note that at 150 mM NaCl, K_1, the affinity of drug for tubulin heterodimers, for all models (Table 3) is 1.2 ($\pm$ 0.2) $\times$ 10^5 M^{-1}, a value extremely similar to our previous results with three *Vinca* alkaloids in 1 mM Mg^{2+} (Lobert et al., 1996). Thus, combining the 100 μM divalent cation data (Fig. 4, Table 3) and the high-salt, 1 mM

divalent cation data (Fig. 5, Table 3) with the NaCl titration data (Figs. 1 and 2, Table 1) and the previous work in the absence of Mg^{2+} (Na and Timasheff, 1986a; Prakash and Timasheff, 1985), we can conclude that *Vinca* alkaloid binding to the tubulin heterodimer is Mg^{2+} or divalent cation dependent but not NaCl dependent in the range of 0–150 mM. This suggests a role for specific divalent cation interactions in drug binding to the heterodimer (see Discussion). (A more extensive study of Mg^{2+} and Ca^{2+} effects under high-salt conditions currently under way should verify and extend these observations.)

CONCLUSION

Ionic strength effects

In the experiments described here, we found that, in the presence of vinblastine or vincristine, NaCl enhances overall association, inducing larger aggregates, while diminishing tubulin precipitation, probably by inhibiting lateral association. At 150 mM NaCl and vinblastine, the GDP enhancement is reduced to less than half that found in the absence of NaCl (equivalent to about 0.24 ± 0.22 kcal/mol compared to 0.75 ± 0.28 kcal/mol for all models). A similar result is found with vincristine-induced association in 150 mM NaCl (0.36 ± 0.10 kcal/mol). Wyman analysis demonstrated a twofold increase in the change in NaCl binding to vinblastine-induced spirals in the presence of GTP compared to GDP. These results suggest that electrostatic effects contribute significantly to the enhancement by GDP, which is probably due to electrostatic repulsion in the GTP-tubulin conformation. A similar electrostatic repulsion is thought to occur in microtubule formation, where high ionic strength favors assembly. This repulsion probably occurs in the highly charged carboxyl tail of both α- and β-tubulin and can be overcome by MAP binding or by subtilisin digestion to remove the acidic region (Lobert et al., 1993). Note that in our previous work with subtilisin-digested tubulin (Lobert and Correia, 1992; Lobert et al., 1993), we observed that the extent and fidelity of cleavage in the carboxyl-tail region of both tubulin chains was dependent upon solution conditions, divalent cation binding, and the extent of tubulin self-association. These results, in conjunction with the thermodynamic linkages in the *Vinca* alkaloid-tubulin system, suggest that salt and divalent cation binding to the carboxyl-tail region is involved in modulating nucleotide and *Vinca* alkaloid-induced self-association events. Note that we are not necessarily referring to a specific binding site or class of binding sites, although there may be a distinction between binding sites for monovalent and divalent cations. Rather, we mean nonspecific interactions in the thermodynamic sense, described as preferential interactions by Timasheff and co-workers (Lee and Timasheff, 1977; Correia, 1991). This is consistent with the small change in the number of NaCl ions (<0.5 mol/mol) associated with the overall affinity K_1K_2 by Wyman analysis. Further note that this linkage corresponds to a single overall association event. During the formation of a spiral a cascade of association events occurs that is linked to a cascade of salt binding events. The recent work by Nogales et al. (1995b) places the carboxyl tail of both α- and β-tubulin near the lateral contacts in Zn-induced sheets and suggests a structural model by which NaCl or other ions might affect lateral interspiral or interprotofilament contacts. These domains are also located between longitudinal subunit interactions and may play a role in spiral formation as well. (Future studies with subtilisin-digested tubulin will provide insight into the involvement of this acidic domain in the linkage between salt or divalent cation binding and tubulin self-association.)

For vinblastine-induced tubulin self-association in the presence of 1 mM Mg^{2+}, K_1 values at 25°C are, within error, identical in the presence or absence of NaCl, 1.2 (± 0.3) × 10^5 M^{-1}, for all models and regardless of nucleotide (Table 1 and Lobert et al., 1995). Thus the affinity of vinblastine for its heterodimer binding site is the same regardless of salt concentration. Similar data collected in the presence of vincristine over a range of NaCl concentrations (0–150 mM NaCl, Table 1 and Lobert et al., 1996) show the same absence of an effect on K_1 (1.6 (± 0.3) × 10^5 M^{-1}) for all models and regardless of nucleotide present. We have previously discussed the insensitivity of K_1 to the *Vinca* alkaloid under investigation in terms of allosteric transitions that can only occur in the spiral polymer form, not in the heterodimer (Lobert et al., 1996). A lack of salt dependence for K_1 suggests that NaCl also affects association events in the polymer and not in the heterodimer. Note that in our previous work (Lobert et al., 1996) the similarity in K_1 between vinblastine, vincristine, and vinorelbine was stressed. Thus GDP enhancement is an effect on K_2, the self-association of liganded heterodimer, or K_3, the drug binding to polymers, and is clearly consistent with linkage between nucleotide binding, drug binding, self-association, and electrostatic effects at distant sites on the tubulin molecule.

Divalent cation effects

Sedimentation velocity studies were conducted with vinblastine and 2 μM tubulin with 100 μM Mg^{2+}, Ca^{2+}, or Mn^{2+} in the absence of NaCl and 1 mM Mg^{2+}, Ca^{2+}, or Mn^{2+} in the presence of NaCl. In the absence of NaCl, we found that 1 mM Mn^{2+} or Ca^{2+} causes immediate condensation of tubulin. The predominant aggregates observed by electron microscopy (negative stain) were large sheets. It is interesting that under both sets of conditions differential divalent cation effects are observed in the GDP but not the GTP solutions. This is in contrast to the effects of NaCl, where the largest effect is observed in the GTP solutions (Fig. 1 and 2). As discussed above, this suggests that NaCl and divalent cations are affecting different regions of the tubulin heterodimer, or are exhibiting differential specificity in their effects on the thermodynamic linkages. Either way, it is clear that their effects are linked to nucleotide binding.

An important conclusion that has emerged from these studies is that K_1, at least for Mg^{2+} and Mn^{2+}, is divalent cation dependent, and yet not NaCl dependent. Wyman analysis was performed by plotting ln K_1 versus ln[M^{2+}] to determine the change in cation binding associated with the binding of drug to the tubulin heterodimer. The slope of this plot, $\Delta\nu$, for the vinblastine data alone corresponds to 0.361 ($\pm$ 0.023) mol/mol, and for the complete vincristine, vinblastine, and vinorelbine data set corresponds to 0.442 ($\pm$ 0.102) mol/mol. This suggests a direct thermodynamic involvement of divalent cations in the binding of *Vinca* alkaloids to the tubulin heterodimer. Although vinblastine and vincristine have two protonatable groups, there is no evidence of direct binding of divalent cations to *Vinca* alkaloids. The *Vinca* alkaloid binding site is reported to be near the exchangeable nucleotide binding site (E-site) on the β-tubulin subunit (Bai et al., 1990) and may be influenced by metal binding to GXP. However, it is well known that GTP binding to the E-site is strongly Mg^{2+} or Mn^{2+} dependent, whereas GDP binding is Mg^{2+} or Mn^{2+} independent (Correia et al., 1987, 1988). Because the effect on K_1 is identical for both GDP and GTP conditions, it is unlikely that a nucleotide-associated metal is directly modifying *Vinca* alkaloid binding to the heterodimer. Thus we can conclude that divalent cation binding to the heterodimer, possibly at some distance, has a direct or indirect thermodynamic effect on K_1, drug association with the *Vinca* alkaloid binding site. Note that, unlike Mg^{2+} and Mn^{2+}, there is no evidence that Ca^{2+} interacts with GTP at the E-site. In the presence of Ca^{2+} and GTP, we assume that Mg^{2+} may not be exchanged and is still present on the GTP-tubulin complex. It is clear that Ca^{2+} does not disrupt GTP binding, because the sedimentation data in the presence of GTP with Ca^{2+}, Mg^{2+}, and Mn^{2+} are all identical within error.

At 100 μM cation, K_1, the binding of the drug to heterodimers, is largest for Ca^{2+} compared to the other two cations (Table 3). In the presence of GTP and Ca^{2+}, K_1 is more than threefold larger than when Mn^{2+} or Mg^{2+} is present. However, when GDP is present the enhancement in K_1 is smaller (less than twofold relative to the other two cations). The increase in K_1 in the presence of Ca^{2+} is partially compensated by a decrease in K_2, the binding of liganded heterodimers to polymers. K_2 is smallest when Ca^{2+} is present compared to when Mn^{2+} or Mg^{2+} is present. Simulations of binding curves demonstrated that K_2 determines the plateau values, and thus smaller K_2 values indicate that smaller polymers are formed, in spite of the fact that the overall affinity, K_1K_2, for all three cations is identical within error (mean 1.6 ($\pm$ 0.1) $\times$ 10^{12} M^{-2}). This result suggests that, relative to other divalent cations, Ca^{2+} can have a regulatory effect on *Vinca* alkaloid-induced spiral formation, because propagation into the GDP microtubule core is less favorable.

We found that 150 mM NaCl suppressed condensation, and so we were able to carry out sedimentation velocity studies with 1 mM cations at high ionic strength. Raising the ionic strength more closely approximates intracellular conditions. Under all of the ionic conditions studied here, differential divalent cation effects are primarily seen in the GDP solutions, suggesting specific ion effects linked to nucleotide binding. Only when GDP and Ca^{2+} are present do we find significantly smaller K_2 values relative to Mn^{2+} and Mg^{2+}. This difference can be seen in the lower plateau values for the Ca^{2+} data (Fig. 5). We can conclude that under low or high ionic strength conditions (near physiological), spiral propagation into the GDP core of the microtubules is less favored by Ca^{2+} compared to Mg^{2+} or Mn^{2+}. Note that the ability of divalent cations to condense *Vinca*-tubulin spirals reported here and by others (Himes et al., 1976; Na and Timasheff, 1986b) is analogous to counterion condensation of DNA or the bundling of actin filaments or microtubules (Tang and Janmey, 1996). Consistent with Manning theory for polyelectrolytes (Manning, 1978; Tang and Janmey, 1996), increased salt concentrations diminish condensation and weaken lateral spiral interactions, thereby raising the concentration of divalent cations needed to induce larger aggregates. This observation suggests that a complete understanding of *Vinca* alkaloid-induced paracrystal formation will require a knowledge of the polyelectrolyte characteristics of tubulin spirals.

Mechanism of *Vinca* alkaloid-induced tubulin self-association

How does ionic strength contribute to the mechanism of *Vinca* alkaloid-induced spiral formation? Stopped-flow light scattering experiments (Fig. 3, Table 2) in the presence of 150 mM NaCl indicate that NaCl diminishes the lateral association of drug-induced spirals. Data collected in the presence of vincristine or vinblastine were best fit with a single exponential, suggesting that similar processes are involved when either drug induces spiral formation. This result differs from our previous report of light scattering experiments with these drugs in the absence of NaCl (Lobert et al., 1996). In those experiments, we found that the vincristine data required two exponentials for adequate fits, suggesting that alignment of spirals occurs in addition to the lengthwise growth of spirals. This was not observed with vinblastine. Thus electrostatic effects contribute to spiral alignment as well as GDP enhancement. Relaxation times overall are much longer when vincristine is present compared to vinblastine, regardless of whether NaCl is present. When 150 mM NaCl is present, relaxation times for vincristine-induced spirals are threefold longer than for vinblastine-induced spirals under the same conditions. This result is consistent with a cascade of events that require more time with the longer vincristine-induced spirals. Furthermore, relaxation times in the presence of vinblastine decrease with increasing protein concentration, indicating oligomer annealing (Lobert et al., 1996). However, the protein concentration dependence is diminished in the presence of NaCl. In fact, the k_{off} and k_{on} estimations result in

a 10-fold smaller K_a compared to the K_2 determined from ligand-mediated fits of sedimentation velocity data. Thus for vinblastine our previous analysis of stopped-flow light scattering data in the absence of NaCl (Lobert et al., 1996) does not appear to be adequate. The protein concentration dependence is not observed with vincristine in the presence or absence of NaCl. It appears that the mechanism of *Vinca* alkaloid-induced tubulin self-association is different when NaCl is present, possibly because of an absence of annealing and/or another rate-limiting step like a conformational change or the release of NaCl. An additional possibility is that in high salt, vinblastine and vincristine induce something other than a single spiral filament. It has been reported that tubulin can also be induced to form double filament spirals (Amos et al., 1984; Hodgkinson et al., 1992; Nogales et al., 1995a). Nogales et al. (1995a) clearly showed that Mg^{2+} concentrations greater than 6 mM favor double filament spirals. In their work, at 1 mM Mg^{2+} and 100 mM PIPES, the spirals were single filaments. Above 6 mM Mg^{2+} they were double filament spirals, and at 6 mM Mg^{2+} there appeared to be an equilibrium between the two forms. This suggests that 10 mM PIPES, ± NaCl, 0.1–1 mM Mg^{2+} would favor single filament spirals. All of the previous work by Timasheff and co-workers (Na and Timasheff, 1986a,b; Prakash and Timasheff, 1985) in 10 mM sodium phosphate, pH 7.0, assumed single-filament spiral formation, a correct assumption in light of the results of Nogales et al. (1995a). Thus we currently have no reason to doubt our choice of mechanism to fit the sedimentation data. Current studies are exploring the influence of higher concentrations of Mg^{2+} and Ca^{2+} on vinblastine-induced spiral formation and may reveal features in the sedimenting boundary shapes or the $g(s)$ profiles that can be interpreted as a conversion from single-filament to double-filament spiral formation.

In vivo consequences of spiral energetics

Our measurements suggest that the thermodynamics of the drug-induced spirals contribute to *Vinca* alkaloid differences in vivo. It has been clearly demonstrated that low *Vinca* alkaloid concentrations kill cells by suppressing microtubule dynamics without depolymerizing microtubules or causing extensive changes in cellular microtubule mass (Dhamodharan et al., 1995). We have speculated, based upon this work, that the energetics of ligand-mediated spiral formation are the parameters clinically relevant for interpreting and modeling therapeutic doses (Lobert et al., 1996). Therefore, our emphasis in this work on spiral formation and the suppression of paracrystal and sheet-like aggregates is sound from the perspective of using the analytical ultracentrifuge as well as extrapolating results to physiological conditions. Vincristine induces longer spirals than vinblastine, and this effect is enhanced at physiological ionic strength. Long polymer distributions reequilibrate more slowly by a mechanism involving a cascade of dissociation events. This is vividly seen in the relaxation times where the larger vincristine polymers have a relaxation time of about 100 s, and the shorter vinblastine polymers have a relaxation time of about 30 s. These results can be correlated with the longer terminal half-life and slower plasma clearance found with vincristine compared to vinblastine (Rahmani et al., 1986; Rowinsky et al., 1994) and may account for the increased neurotoxicity for vincristine relative to vinblastine and vinorelbine. Thus in vivo differences between vinblastine and vincristine can be attributed in part to slower kinetics of redistribution. In fact, vinorelbine, which has the lowest potential for toxicity, forms the smallest polymers (Lobert et al., 1996) and consequently has the fastest relaxation times, about 10 s. Moreover, in the presence of vincristine or vinblastine, we have observed divalent cation differences in association constants and kinetics that may be determined by divalent cation interactions with sites on the carboxyl terminus. Changes in cell membranes associated with low plasma magnesium levels and mobilization of extracellular and intracellular calcium have been implicated in oncogenesis (reviewed in Kummerow, 1992; Battistini et al., 1993), and hypercalcemia is commonly observed in cancer patients, possibly because of altered humoral factors and/or increased bone resorption (Hoekman and Tjandra, 1991; reviewed in Kaplan, 1994). Thus clinically important changes in intracellular and extracellular calcium or magnesium concentrations may affect the activity of chemotherapeutic agents like *Vinca* alkaloids. We further recognize the potential role of polyglutamylation, a post-translational modification that occurs in the carboxyl-tail region of both tubulin polypeptide chains (Alexander et al., 1991; Redeker et al., 1992; Rudiger et al., 1992). Tissue-specific differences in polyglutamylation may contribute to *Vinca* alkaloid efficacy and toxicity. We are currently investigating these possibilities using subtilisin-cleaved tubulin heterodimers and tubulin isolated from tissues in which polyglutamylation is known to be minimal.

This work was supported by grants NR00056 (SL) and BIR9216150 (JJC).

REFERENCES

Alexander, J. E., D. F. Hunt, M. K. Lee, J. Shabanowitz, H. Michel, S. C. Berlin, T. L. MacDonald, R. J. Sundberg, L. I. Rebhun, and A. Frankfurter. 1991. Characterization of posttranslational modifications in neuron-specific class III β-tubulin by mass spectrometry. *Proc. Natl. Acad. Sci. USA.* 88:4685–4689.

Amos, L. A., J. S. Jubb, R. Henderson, and G. Vigers. 1984. Arrangement of protofilaments in two forms of tubulin crystals induced by vinblastine. *J. Mol. Biol.* 178:711–729.

Bai, R., G. R. Pettit, and E. Hamel. 1990. Binding of dolastatin 10 to tubulin at a distinct site for the peptide antimitotic agents near the exchangeable nucleotide and *Vinca* alkaloid sites. *J. Biol. Chem.* 265: 17141–17149.

Battistini, B., P. Chailler, P. D'Orleans-Juste, N. Briere, and P. Sirois. 1993. Growth regulatory properties of endothelins. *Peptides.* 14: 385–399.

Berkowitz, S. A., and J. Wolff. 1981. Intrinsic calcium sensitivity of tubulin polymerization. *J. Biol. Chem.* 256:11216–11223.

Correia, J. J. 1991. Effects of antimitotic agents on tubulin-nucleotide interactions. *Pharmacol. Ther.* 52:127–147.

Correia, J. J., L. T. Baty, and R. C. Williams, Jr. 1987. Mg^{2+} dependence of guanine nucleotide binding to tubulin. *J. Biol. Chem.* 262: 17278–17284.

Correia, J. J., A. H. Beth, and R. C. Williams, Jr. 1988. Tubulin exchanges divalent cations at both guanine nucleotide-binding sites. *J. Biol Chem.* 263:10681–10686.

Detrich, H. W., and R. C. Williams, Jr. 1978. Reversible dissociation of the $\alpha\beta$ dimer of tubulin from bovine brain. *Biochemistry.* 17:3900–3907.

Dhamodharan, R., M. A. Jordan, D. Thrower, L. Wilson, and P. Wadsworth. 1995. Vinblastine suppresses dynamics of individual microtubules in living interphase cells. *Mol. Biol. Cell.* 6:1215–1229.

Frigon, R. P., and S. N. Timasheff. 1975a. Magnesium-induced self-association of calf brain tubulin. I. Stoichiometry. *Biochemistry.* 14: 4559–4566.

Frigon, R. P., and S. N. Timasheff. 1975b. Magnesium-induced self-association of calf brain tubulin. II. Thermodynamics. *Biochemistry.* 14:4567–4573.

Himes, R. 1991. Interactions of the catharanthus (*Vinca*) alkaloids with tubulin and microtubules. *Pharmacol. Ther.* 51:257–267.

Himes, R. H., R. N. Kersey, I. Heller-Bettinger, and F. E. Samson. 1976. Action of the *Vinca* alkaloids vincristine, vinblastine, and desacetyl vinblastine amide on microtubules in vitro. *Cancer Res.* 36:3798–3802.

Hodgkinson, J. L., T. Hutton, F. J. Medrano, and J. Bordas. 1992. X-ray solution scattering on vinblastine-induced polymers of microtubule protein: structural characterization and effects of temperature. *J. Struct. Biol.* 109:28–38.

Hoekman, K., and Y. I. Tjandra. 1991. The role of 1,25-dihydroxyvitamin D in the maintenance of hypercalcemia in a patient with an ovarian carcinoma producing parathyroid hormone-related protein. *Cancer.* 68: 642–647.

Howard, W. D., and S. N. Timasheff. 1986. GDP state of tubulin: stabilization of double rings. *Biochemistry.* 25:8929–8300.

Kaplan, M. 1994. Hypercalcemia of malignancy: a review of advances in pathophysiology. *Oncol. Nurs. Forum.* 21:1039–1046.

Kummerow, F. A. 1992. Hypothesis: possible role of magnesium and calcium in the development of structure and function of the plasma membrane in mammalian cells and in human diseases. *J. Am. Coll. Nutr.* 11:410–425.

Lee, J. C., and S. N. Timasheff. 1977. In vitro reconstitution of calf brain microtubules: effects of solution variables. *Biochemistry.* 16: 1754–1764.

Liu, S., and W. F. Stafford, III. 1995. An optical thermometer for direct measurement of cell temperature in the Beckman instruments XL-A analytical ultracentrifuge. *Anal. Biochem.* 224:199–202.

Lobert, S., and J. J. Correia 1992. Subtilisin cleavage of tubulin heterodimers and polymers. *Arch. Biochem. Biophys.* 296:152–160.

Lobert, S., A. Frankfurter, and J. J. Correia. 1995. Binding of vinblastine to phosphocellulose-purified and $\alpha\beta$-class III tubulin: the role of nucleotides and β-tubulin isotypes. *Biochemistry.* 34:8050–8060.

Lobert, S., B. S. Hennington, and J. J. Correia. 1993. Multiple sites for subtilisin cleavage of tubulin: effects of divalent cations. *Cell Motil. Cytoskel.* 25:282–297.

Lobert, S., B. Vulevic, and J. J. Correia. 1996. Interaction of *Vinca* alkaloids with tubulin: a comparison of vinblastine, vincristine and vinorelbine. *Biochemistry.* 35:6806–6814.

Manning, G. S. 1978. The molecular theory of polyelectrolyte solutions with applications to the electrostatic properties of polynucleotides. *Q. Rev. Biophys.* II:179–246.

Na, G. C., and S. N. Timasheff. 1985. Measurement and analysis of ligand-binding isotherms linked to protein self-association. *Methods Enzymol.* 117:459–495.

Na, G. C. and, S. N. Timasheff. 1986a. Interaction of vinblastine with calf brain tubulin: multiple equilibria. *Biochemistry.* 25:6214–6222.

Na, G. C., and S. N. Timasheff. 1986b. Interaction of vinblastine with calf brain tubulin: effect of magnesium ion. *Biochemistry.* 25:6222–6228.

Nogales, E., F. J. Medrano, G. P. Diakun, G. R. Mant, E. Towns-Andrews, and J. Bordas. 1995a. The effect of temperature on the structure of vinblastine-induced polymers of purified tubulin: detection of a reversible conformation change. *J. Mol. Biol.* 254:416–430.

Nogales, E., S. G. Wolf, I. A. Khan, R. L. Ludueña, and K. H. Downing. 1995b. Structure of tubulin at 6.5 Å and location of the taxol-binding site. *Nature.* 375:424–427.

Prakash, V., and S. N. Timasheff. 1985. Vincristine-induced self-association of calf brain tubulin. *Biochemistry.* 24:5004–5010.

Rahmani, R., F. Gueritte, M. Martin, S. Just, J. P. Cano, and J. Barbet. 1986. Comparative pharmacokinetics of antitumor *Vinca* alkaloids; intravenous bolus injections of navelbine and related alkaloids to cancer patients and rats. *Cancer Chemother. Pharmacol.* 16:223–228.

Redeker, V., R. Melki, D. Prome, J. P. Le Caer, and J. Rossier. 1992. Structure of tubulin C-terminal domain obtained by subtilisin treatment. *FEBS Lett.* 313:185–192.

Rowinsky, E. K., D. A. Noe, D. L. Trump, E. P. Winer, V. S. Lucas, W. A. Wargin, J. A. Hohneker, B. Lubejko, S. E. Sartorius, D. S. Ettinger, and R. C. Donehower. 1994. Pharmacokinetic, bioavailability and feasibility study of oral vinorelbine in patients with solid tumors. *J. Clin. Oncol.* 12:1754–1763.

Rudiger, M., U. Plessman, K. D. Kloppel, J. Wehland, and K. Weber. 1992. Class II tubulin, the major brain β tubulin isotype is polyglutamylated on glutamic acid residue 435. *FEBS Lett.* 308:101–105.

Serrano, L., J. E. Dominguez, and J. Avila. 1988. Identification of zinc-binding sites of proteins: zinc binds to the amino-terminal region of tubulin. *Anal. Biochem.* 172:210–218.

Serrano, L., A. Valencia, R. Caballero, and J. Avila. 1986. Localization of the high affinity calcium-binding site on tubulin molecule. *J. Biol. Chem.* 261:7076–7081.

Singer, W. D., R. T. Hersh, and R. H. Himes. 1988. Effects of solution variables on the binding of vinblastine to tubulin. *Biochem. Pharmacol.* 37:2691–2696.

Stafford, W. F., III. 1992a. Boundary analysis in sedimentation transport experiments: a procedure for obtaining sedimentation coefficient distributions using the time derivative of the concentration profile. *Anal. Biochem.* 203:295–301.

Stafford, W. F., III. 1992b. Methods for obtaining sedimentation coefficient distributions. *In* Analytical Ultracentrifugation in Biochemistry and Polymer Sciences. S. E. Harding, A. Rowe, and J. C. Horton, editors. Royal Society of Chemistry, Cambridge, England. 359–393.

Stafford, W. F., III. 1994. Boundary analysis in sedimentation velocity experiments. *In* Methods in Enzymology. Numerical Computer Methods, Part B. 240. M. L. Johnson and L. Brands, editors. Academic Press, New York. 478–501.

Tang, J. X., and P. A. Janmey. 1996. The polyelectrolyte nature of F-actin and the mechanism of actin bundle formation. *J. Biol. Chem.* 271: 8556–8563.

Thusius, D., P. Dessen, and J. M. Jallon. 1975. Mechanism of bovine liver glutamate dehydrogenase self-association. I. Kinetic evidence for a random association of polymer chains. *J. Mol. Biol.* 92:413–432.

Williams, R. C., Jr., and J. C. Lee. 1982. Preparation of tubulin from brain. *Methods Enzymol.* 85:376–408.

Wilson, L., J. Bryan, A. Ruby, and D. Mazia. 1970. Precipitation of proteins by vinblastine and calcium ions. *Proc. Natl. Acad. Sci. USA.* 66:807–814.

Wyman, J. 1964. Linked functions and reciprocal effects in hemoglobin: a second look. *Adv. Protein Chem.* 19:223–386.